Nonlinear Dynamics manuscript No.
(will be inserted by the editor)

Optimisation of chaotically perturbed acoustic limit cycles

Francisco Huhn · Luca Magri*

Abstract In an acoustic cavity with a heat source, the thermal energy of the heat source can be converted into acoustic energy, which may generate a loud oscillation. If uncontrolled, these acoustic oscillations, also known as thermoacoustic instabilities, can cause mechanical vibrations, fatigue and structural failure. The objective of manufacturers is to design stable thermoacoustic configurations. In this paper, we propose a method to optimise a chaotically perturbed limit cycle in the bistable region of a subcritical bifurcation. In this situation, traditional stability and sensitivity methods, such as eigenvalue and Floquet analysis, break down. First, we propose covariant Lyapunov analysis and shadowing methods as tools to calculate the stability and sensitivity of chaotically perturbed acoustic limit cycles. Second, covariant Lyapunov vector analysis is applied to an acoustic system with a heat source. The acoustic velocity at the heat source is chaotically perturbed to *qualitatively* mimic the effect of the turbulent hydrodynamic field. It is shown that the tangent space of the acoustic attractor is hyperbolic, which has a practical implication: the sensitivities of time–averaged cost functionals exist and can be robustly calculated by a shadowing method. Third, we calculate the sensitivities of the time–averaged acoustic energy and Rayleigh index to small changes to the heat–source intensity and time delay. By embedding the sensitivities into a gradient–update routine, we suppress an existing chaotic acoustic oscillation by optimal design of the heat source. The analysis and methods proposed enable the reduction of chaotic oscillations in thermoacoustic systems by optimal passive control. Because the theoretical framework is general, the techniques presented can be used in other unsteady *deterministic multi-physics* problems with virtually no modification.

1 Introduction

Gas-turbine and rocket-motor manufacturers strive to design engines that do not experience thermoacoustic instabilities [1, 2, 3, 4, 5]. Thermoacoustic instabilities

* Corresponding author, E-mail: lm547@cam.ac.uk

Cambridge University Engineering Department, Trumpington Street, Cambridge CB2 1PZ, UK

occur when the heat released by the flame is sufficiently in phase with the acoustic pressure [6] such that the thermal energy of the flame that is converted into acoustic energy exceeds dissipation mechanisms. The first objective of manufacturers is to design a thermoacoustic system in which small acoustic perturbations decay after some time, i.e. all the eigenvalues are stable. Eigenvalue analysis is routinely used in industrial preliminary design and parametric studies because it can be run quickly [e.g., 1]. However, when nonlinearities become active, thermoacoustic systems exhibit rich behaviours both via supercritical bifurcations, i.e., when an eigenvalue becomes unstable, and subcritical bifurcations, i.e., when eigenvalues are stable but the nonlinearity is triggered by a finite-amplitude acoustic perturbation. When the bifurcation parameter is varied, thermoacoustic systems may display periodic, quasi periodic and chaotic oscillations [7, 8, 9, 10, 11, 12, 13, 14, 15]. Chaotic acoustic oscillations originate from two main physical nonlinearities, which are deterministic:

1. The heat released by the flame is a nonlinear function of the acoustic perturbations at the flame's base, i.e. the flame saturates nonlinearly [16, 17]. Both experimental investigations [7, 8, 9, 10] and numerical studies [11, 12, 14] showed that the nonlinear flame saturation may cause an acoustic limit cycle to become chaotic, by either period doubling, or Ruelle-Takens-Newhouse, or intermittency scenarios [13, 15], which are common to other fluid dynamics systems [18, 19, 20]. The numerical studies of Kashinath et al. [11], Waugh et al. [12], Orchini et al. [14] showed that the nonlinear flame saturation may generate chaotic acoustic oscillations even in laminar flame models, where the turbulent hydrodynamics is not modelled. The optimisation of this type of chaotic oscillations was proposed by Huhn and Magri [21].
2. The geometry of the combustor promotes hydrodynamic instabilities, such as vortex shedding and shear-layer instabilities [22], which result in energetic coherent structures. In turbulent combustors, turbulence unpredictably perturbs the dynamics of coherent structures, which, in turn, unpredictably perturb the flame dynamics, thereby changing the heat release that feeds into the acoustics.

The objective of this paper it to generalise the method of [21] to tackle both nonlinear sources 1-2. We showcase the proposed method for the optimisation of chaotic oscillations of type 2.

Such unpredictable and erratic behaviours can be physically *modelled* as noise. Stochastic models have been proposed in thermoacoustics to determine the linear growth rate by system identification of raw signals [e.g., 23, 24, 25]; and to phenomenologically model the turbulent hydrodynamics to capture the intermittent bursts that occur before thermoacoustic instabilities [13, 26]. On the one hand, stochastic methods are particularly well suited to dealing with experimental data, which are contaminated by random disturbances and uncertainties, such as those from the environment and instrumentation. On the other hand, the thermoacoustic problem is governed by the compressible Navier-Stokes equations equipped with energy, continuity and chemistry equations. These equations are *deterministic*: For exactly the same parameters and initial / boundary conditions, the solution is unique (if it exists). However, because of the chaotic nature of these flows, almost every small perturbation to the systems exponentially diverges [27] and the instantaneous solutions will be completely different after a characteristic time, which scales with the inverse of the maximal Lyapunov exponent [e.g., 28, 29, 30]. This

extreme sensitivity to small perturbations is popularly known as the "butterfly effect" [31]. From a dynamical systems perspective, the turbulent hydrodynamic field, which changes the heat-release dynamics, is deterministic and unpredictable, i.e., it is chaotic. Indeed, large-eddy simulations, which solve deterministic equations, showed that the power density spectrum of turbulent combustors during thermoacoustic instability has a high peak centred around the most excited acoustic frequency with a broadband content [e.g., 32, 33, 34]. Importantly, laboratory experiments have shown that thermoacoustic systems behave like deterministic systems when they become unstable, as thoroughly reviewed in Section 4.2 of Juniper and Sujith [5]. This experimental evidence has recently motivated the use of tools from dynamical systems theory for the analysis of chaotic thermoacoustic oscillations, such as nonlinear time series analysis [9, 10, 35], multi-fractal analysis and Hurst exponents [13, 36], complex networks [37], synchronisation theory [38, 39], to name only a few.

Although oscillations in thermoacoustic systems may be nonlinear and chaotic, industrial preliminary design is based on linear analysis [1, 5]: the first objective is to design eigenvalue-stable thermoacoustic systems. Sensitivity methods have recently been developed to calculate the effect that a small change to the system has on the eigenvalue. Sensitivity analysis [40] quantitatively informs the practitioner, among others, on (i) how to optimally change design parameters, such as geometric quantities [41]; (ii) which passive device is most stabilising [42]; and (iii) how large is the uncertainty of the stability calculations [43, 44, 45]. When the gradient provided by sensitivity analysis is embedded into an optimisation routine, it is possible to calculate the optimal arrangement of acoustic dampers [46] and a stable set of geometric parameters [47]. However, eigenvalue analysis is necessary but not sufficient to prevent large acoustic oscillations. This is the case of subcritical bifurcations, where the system can self-sustain finite-amplitude oscillations in the bistable region, where all eigenvalues are stable. In this paper, the focus is on deterministic systems. We provide a method to calculate the sensitivity of chaotic acoustic oscillations to stabilise a nonlinearly unstable, yet eigenvalue-stable, thermoacoustic system. Therefore, we regard the action of turbulence as that of chaotically perturbing an acoustic limit-cycle. Hence, we propose a *qualitative* reduced order model of a chaotically perturbed limit cycle to test the optimisation method that we propose.

The paper is structured as follows. Section 2 introduces the theoretical framework and tools for the optimisation of *time-averaged* cost functionals in chaotic thermoacoustic systems. Section 3 presents the *qualitative* reduced order model of a chaotically perturbed limit cycle. In Section 4, a covariant Lyapunov vector analysis is performed to analyse the hyperbolic behaviour of the system. The sensitivities of two key time-averaged thermoacoustic cost functionals (acoustic energy and Rayleigh index) are calculated via a shadowing method and numerically verified in Section 5. In Section 6, the sensitivities are embedded into a gradient-update algorithm to compute the optimal change to the design parameters to suppress a chaotically perturbed limit cycle.

2 Sensitivity of time-averaged cost functionals in chaotic systems

In chaotic oscillations, a quantity of interest that we wish to optimise is the time average of a cost functional, $\mathcal{J}$

$$\langle \mathcal{J}(\boldsymbol{s}) \rangle \triangleq \lim_{T\to\infty} \frac{1}{T} \int_0^T \mathcal{J}(\boldsymbol{s}; \boldsymbol{q}(t)) dt, \tag{1}$$

where $\boldsymbol{q}$ is the state vector, t is the time, $\langle \cdot \rangle$ represents the time average operation, which is equal to the expected value in ergodic systems (Birkhoff ergodic theorem [48]), and $\boldsymbol{s}$ is the parameters' vector. Physically, $\mathcal{J}$ may be an acoustic energy, which we want to minimise to make the combustor operate in stable conditions. Therefore, the objective is to calculate the sensitivity of the time-averaged cost functional given a perturbation to the parameters' vector, i.e. $\nabla_{\boldsymbol{s}} \langle \mathcal{J} \rangle$. Whereas sensitivity analysis of eigenvalues is robust, traditional sensitivity methods fail in chaotic systems because of the butterfly effect [49]. The gradient of the time-averaged cost functional (1) explicitly reads

$$\nabla_{\boldsymbol{s}} \langle \mathcal{J} \rangle \triangleq \frac{d}{d\boldsymbol{s}} \left(\lim_{T\to\infty} \frac{1}{T} \int_0^T \mathcal{J}(\boldsymbol{s}; \boldsymbol{q}(t)) dt \right). \tag{2}$$

In a chaotic attractor, the operations of differentiation and time average do not commute, i.e., $\nabla_{\boldsymbol{s}} \langle \mathcal{J} \rangle \neq \langle \nabla_{\boldsymbol{s}} \mathcal{J} \rangle$, where

$$\langle \nabla_{\boldsymbol{s}} \mathcal{J} \rangle = \lim_{T\to\infty} \frac{1}{T} \int_0^T \left(\frac{\partial \mathcal{J}}{\partial \boldsymbol{s}} + \frac{\partial \mathcal{J}}{\partial \boldsymbol{q}} \frac{\partial \boldsymbol{q}}{\partial \boldsymbol{s}} \right) dt. \tag{3}$$

The term $\partial \boldsymbol{q}/\partial \boldsymbol{s}$ can be thought as the distance between a trajectory obtained with $\boldsymbol{s} = \boldsymbol{s}_0$ and another trajectory $\boldsymbol{s} = \boldsymbol{s}_0 + \delta \boldsymbol{s}$. In chaotic systems, it grows exponentially, rendering $\langle \nabla_{\boldsymbol{s}} \mathcal{J} \rangle$ unbounded. This behaviour is observed in small systems with at least three degrees of freedom [31], to large-scale turbulent simulations with tens or hundreds of millions of degrees of freedom [30].

The unboundedness of (3) can be avoided with the use of ensemble methods [50], which consist in applying (3) to short trajectories, before $\partial \boldsymbol{q}/\partial \boldsymbol{s}$ becomes too large. The result is then the average of the results of the various trajectories. However, these methods suffer from low rate of convergence. A more efficient alternative to ensemble methods that has been recently proposed to carry out sensitivity analysis of chaotic systems is the class of shadowing methods [51, 52, 53, 54]. By noting that changing a parameter of a chaotic system has a similar effect to changing the initial condition, shadowing methods find a perturbed (shadow) trajectory that does not diverge from the unperturbed trajectory. Such a trajectory is guaranteed to exist by the Shadowing Lemma [e.g., 55, 56, 57] and the sensitivity calculation is enabled because the expectation (1) is a smooth function of the parameters in hyperbolic dynamical systems, as explained in Ruelle's linear theory [58]. A hyperbolic strange attractor is an invariant set whose tangent space can be decomposed in stable, unstable and neutrally stable subspaces, E^u, E^n, E^s, respectively, at almost every point. One basis for this decomposition consists of the covariant Lyapunov vectors [59, 60]. Hyperbolic attractors are also ergodic and, importantly, they have differentiable expectations [58], $\langle \mathcal{J} \rangle$, whereas non-hyperbolic

systems may not. Thus, the sensitivities of time-averaged cost functionals are well-defined in hyperbolic systems, but may be ill-defined in non-hyperbolic systems. For chaotic sensitivity methods to work in thermoacoustics, it is crucial that the hyperbolicity assumption is verified.

2.1 Numerical verification of hyperbolicity

In order to verify hyperbolicity in a numerical simulation, the method described in Takeuchi et al. [61] is used here. The angles between the three pairs of subspaces, $\theta_{u,n} = \angle(E^u, E^n)$, $\theta_{u,s} = \angle(E^u, E^s)$, $\theta_{n,s} = \angle(E^n, E^s)$, are computed. These angles are computed by using the principal angles, $\cos\left(\theta_{A,B}\right) = \bar{\sigma}(\boldsymbol{Q}_A \boldsymbol{Q}_B)$, where matrices $\boldsymbol{Q}_A$ and $\boldsymbol{Q}_B$ define the orthonormal bases of any subspaces A and B (not only E^u, E^n, E^s), respectively, and $\bar{\sigma}$ is the largest singular value. Then, a probability density function of each of these angles is extracted via a histogram of the time series. The system behaves hyperbolically if there are no tangencies between the subspaces, i.e. the value of the probability density functions at $\theta = 0$ is 0.

2.2 Lyapunov exponents and covariant Lyapunov vectors

This section introduces the key concepts to perform stability and sensitivity analysis of chaotic thermoacoustic systems. In particular, we present the key results of Oseledets' theorem [62] to lay out the fundamentals of covariant Lyapunov vector analysis [60]. The thermoacoustic problem is governed by partial differential equations, i.e., the compressible Navier-Stokes equation with equations for the chemistry, and mass and energy conservation. After spatial discretisation, the thermoacoustic problem is formally an autonomous dynamical system

$$\begin{cases} \dot{\boldsymbol{q}}(t) = \boldsymbol{F}(\boldsymbol{q}(t)) \\ \boldsymbol{q}(0) = \boldsymbol{q}_0 \end{cases}, \tag{4}$$

where the overdot $\dot{(\,)}$ is Newton's notation for time differentiation; $\boldsymbol{q} \in \mathbb{R}^N$ is the state vector (e.g., pressure and velocity at each discrete location), where the integer N denotes the discrete degrees of freedom; the subscript 0 denotes the initial condition; and $\boldsymbol{F} : \mathbb{R}^N \to \mathbb{R}^N$ is a nonlinear smooth function, which encapsulates the discretised boundary conditions. We are interested in the evolution of small perturbations, therefore we split the solution as

$$\boldsymbol{q}(t) = \bar{\boldsymbol{q}}(t) + \boldsymbol{q}'(t), \tag{5}$$

where $\bar{\boldsymbol{q}}(t)$ is the unperturbed solution of (4), and $\boldsymbol{q}'(t)$ is the small perturbation such that $||\boldsymbol{q}'(t)||/||\bar{\boldsymbol{q}}(t)|| \sim O(\epsilon)$, where $\epsilon \to 0$. The perturbation is governed by the tangent equation

$$\begin{cases} \dot{\boldsymbol{q}}' = \boldsymbol{J}(t)\boldsymbol{q}', \\ \boldsymbol{q}'(0) = \boldsymbol{q}'_0, \end{cases} \tag{6}$$

where $\boldsymbol{J}(t) \equiv \frac{d\boldsymbol{F}}{d\boldsymbol{q}}\big|_{\bar{\boldsymbol{q}}(t)}$ is the Jacobian. To define the Lyapunov exponents, it is convenient to introduce the tangent propagator, which maps the perturbation, $\boldsymbol{q}'$, from time t to time $t+\tilde{t}$, as

$$\boldsymbol{q}'(t+\tilde{t}) = \boldsymbol{M}(t,\tilde{t})\boldsymbol{q}'(t). \tag{7}$$

The tangent propagator is governed by the matrix equation

$$\begin{cases} \frac{d\boldsymbol{M}}{d\tilde{t}} = \boldsymbol{J}(\tilde{t})\boldsymbol{M}, \\ \boldsymbol{M}(t,0) = \boldsymbol{I}, \end{cases} \tag{8}$$

where $\boldsymbol{I}$ is the identity matrix. Setting $t=0$ without loss of generality, the norm of an infinitesimal perturbation, $\boldsymbol{q}'_0$, to the initial condition, $\bar{\boldsymbol{q}}_0$, asymptotically grows (or decays) as

$$||\boldsymbol{q}'(\tilde{t})|| \cong ||\boldsymbol{q}'_0|| e^{\lambda(\boldsymbol{q}'_0,\bar{\boldsymbol{q}}_0)\tilde{t}}, \tag{9}$$

where $\cong$ means "asymptotically equal to", and

$$\lambda(\boldsymbol{q}'_0,\bar{\boldsymbol{q}}) = \lim_{\tilde{t}\to\infty} \frac{1}{\tilde{t}} \log \frac{||\boldsymbol{M}(0,\tilde{t})\boldsymbol{q}'_0||}{||\boldsymbol{q}'_0||} \tag{10}$$

is the characteristic Lyapunov exponent. Oseledets' theorem [62] shows that there exist N Lyapunov exponents $\lambda_1 \geq \lambda_2 \geq \cdots \geq \lambda_N$, which are constants of the attractor. A Lyapunov exponent corresponds to an unstable / neutral / stable mode if it is positive / neutral / negative. The Lyapunov exponents are the average exponential contraction/expansion rates of an infinitesimal volume of the phase space moving along the attractor. On the one hand, if the attractor is a fixed point, the Lyapunov exponents are equal to the real part of the eigenvalues of the Jacobian at the fixed point; on the other hand, if the attractor is a limit cycle, the Lyapunov exponents are equal to the real part of the Floquet exponents [21]. A chaotic system has at least one positive Lyapunov exponent.

To each Lyapunov exponent, λ_j, there is an associated covariant Lyapunov vector, $\boldsymbol{\phi}_j$. If $\boldsymbol{q}'_0$ is decomposed in the basis of all the covariant Lyapunov vectors, $\{\boldsymbol{\phi}_1,\cdots,\boldsymbol{\phi}_N\}$, the ratio in the argument of the logarithm of (10) is dominated by the largest non-zero component of the decomposition. Consequently, $\lambda(\boldsymbol{q}'_0,\bar{\boldsymbol{q}}) = \lambda_j$, where j is the index of the first non-zero component of $\boldsymbol{q}'_0$ in the covariant Lyapunov vector basis. Furthermore, it can be shown [21] that a bounded covariant Lyapunov vector, $\boldsymbol{\phi}$, associated to a Lyapunov exponent, λ, is governed by

$$\frac{d\boldsymbol{\phi}}{d\tilde{t}} = \boldsymbol{J}\boldsymbol{\phi} - \lambda\boldsymbol{\phi}. \tag{11}$$

Equation (11) illustrates that a covariant Lyapunov vector is evolved by the tangent system, with the second term on the right-hand side ensuring that it stays bounded. Figure 1 pictorially describes the evolution of perturbations in the direction of different covariant Lyapunov vectors. Three covariant Lyapunov vectors are shown at two different instants, each associated with a different Lyapunov exponent, which can be positive, zero or negative along the unstable (red), neutral (orange) and stable (green) covariant Lyapunov vectors, respectively. The resulting perturbed trajectories (dashed lines), converge, stay constant or diverge, respectively, to/from the unperturbed trajectory, depending on the sign of the Lyapunov

exponent. This explains why trajectories emanating from two very close initial conditions will almost surely diverge in chaotic systems – it is highly unlikely for the vector connecting the two initial conditions not to have a component in the direction of the unstable covariant Lyapunov vector.

3 Chaotic thermoacoustic model

We present a model of a chaotic thermoacoustic system, which consists of coupling a generator of chaotic disturbances that perturb the acoustic velocity of a nonlinear heat-release model (Figure 2). The acoustics are longitudinal and governed by the linearised Euler equations. The chaotic perturbation is provided by the Lorenz system, which behaves like a hyperbolic chaotic system to *qualitatively* mimic the effect of the hydrodynamic field. The chaotic model does not attempt to quantitatively reproduce a turbulent hydrodynamic field – this is not the objective. The objective is to capture the essential dynamical systems feature of the chaotic perturbation induced by the hydrodynamics, which is hyperbolic chaos (Section 1). The stability, sensitivity and optimisation framework presented in this paper can be used in more realistic hydrodynamic models[1] with virtually no modification.

[1]For example, in large-eddy simulations, the nonlinear operator $\boldsymbol{F}$ in the dynamical system formulation in Eq. (4) is provided by the spatial discretisation of the momentum, mass and energy conservation laws and chemistry equations [63].

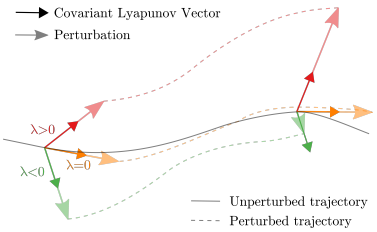

Fig. 1: Schematic diagram of covariant Lyapunov vectors and perturbations on an unperturbed trajectory.

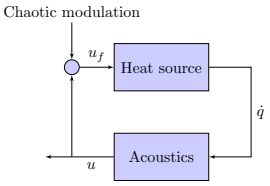

Fig. 2: Schematic of the chaotic thermoacoustic model.

3.1 Lorenz system

The Lorenz system [31] consists of a set of three nonlinear ordinary differential equations

$$\begin{aligned} \dot{x}_L &= \sigma_L(y_L - x_L) \\ \dot{y}_L &= x_L(\rho_L - z_L) - y_L \\ \dot{z}_L &= x_L y_L - \beta_L z_L, \end{aligned} \tag{12}$$

where the variables, x_L, y_L, z_L, and positive parameters $\sigma_L = 10, \rho_L = 8/3, \beta_L = 28$ are used to generate a chaotic signal [64] to perturb the velocity at the heat source (Section 3.2). Mathematically, the Lorenz system has some key properties that are shared by several high dimensional systems. It is chaotic, i.e. it produces unpredictable dynamics; and for the range of parameters we use, it is quasi-hyperbolic [65, 66], which means that it behaves like a hyperbolic system for the purpose of this analysis [53, 67]. These two conditions fulfil the chaotic hypothesis[2], which holds in high-dimensional fluids systems. Because of its properties, the Lorenz system is used as a prototypical system in a wide range of fundamental studies on chaos [e.g. 29, 71, 72] and in the development of new computational methods [e.g. 51, 52, 53]. Instead of being a generator of stochastic dynamics, it is a generator of synthetic chaos[3].

3.2 Acoustics and heat source

A thermoacoustic system consists of three subsystems that interact with each other: the acoustics, flame and hydrodynamics [22, 40]. The acoustics strongly depend on the geometry of the configuration and the boundary conditions. The flame is governed by chemistry mechanisms and their interaction with the turbulent environment. The hydrodynamics is governed by the geometry of the inlets and flame holders, which generate large coherent structures due to flow instabilities (vortex shedding, shear layer instabilities, etc.), which, in turn, are perturbed by turbulence. To accurately model thermoacoustic instabilities, high-fidelity simulations can be employed [e.g., 4]. However, in this fundamental paper, we aim at capturing the essential physical mechanisms of chaotic thermoacoustic instabilities. Therefore, we choose a prototypical time-delayed thermoacoustic system with a longitudinal acoustic cavity and a heat source modelled with a time-delayed model. The main assumptions are: (i) the acoustics are small perturbations onto a low-Mach number mean flow with uniform density; (ii) viscosity and diffusivity are negligible; and (iii) the acoustics are one-dimensional, i.e. the cut-on frequency of the duct is much higher than the frequency of the instability. Under these assumptions, the linearisation of the inviscid momentum and energy equations yields,

[2]It has been hypothesised by Gallavotti and Cohen [68], Gallavotti [69] that most high-dimensional physical systems develop asymptotically on an attracting set, the dynamics of which can be regarded as hyperbolic. This is called the *chaotic hypothesis*, which stems from measure theory of turbulence of [70].

[3]This paper provides a method to optimise deterministic thermoacoustic systems. Including stochastic processes in the optimisation of chaotic thermoacoustic systems is beyond the scope of this paper and is left for future work.

respectively [42, 73, 74]

$$\frac{\partial u}{\partial t} + \frac{\partial p}{\partial x} = 0 \tag{13}$$

$$\frac{\partial p}{\partial t} + \frac{\partial u}{\partial x} + \zeta p - \dot{q}\delta(x - x_f) = 0, \tag{14}$$

where u, p, $\dot{q}$, x and t are the non-dimensional velocity, pressure, heat-release rate, axial coordinate and time, respectively. The reference scales for speed, pressure, length and time are the mean-flow convection velocity, the mean-flow Mach number multiplied by the heat capacity factor, the length of the tube, and the length of the tube divided by the mean-flow speed of sound, respectively. The damping coefficient, ζ, takes into account all the acoustic dissipation (Section 3.2.2). The duct has open ends, which means that the acoustic pressure is zero at the boundaries. The spatial extent of the heat source is assumed negligible as compared to the acoustic wavelength [16], thus, it is modelled as a compact source of acoustic energy through a Dirac delta (generalised) function, $\delta(x - x_f)$ localised at $x_f = 0.3$. The heat-release rate is provided by a modified King's law [75, 76, 77, 78, 79]

$$\dot{q}(t) = \beta\left[\left(1 + u_f(t-\tau)\right)^{\frac{1}{2}} - 1\right], \tag{15}$$

which is a nonlinear time-delayed model for an electrically heated wire. In this paper, $\beta = 0.82$ and $\tau = 0.04$, except where stated otherwise. This model has similar features to flame models, such as the n-τ model [e.g., 5]. Because Lyapunov analysis is valid only for smooth dynamical systems, we approximate the heat-release law (15) by a fourth-degree polynomial in a small neighbourhood of $u_f(t-\tau) = -1$, which enables continuity of both the function and its derivative, to make the derivative smooth [21]. The heat parameter, β, and time delay, τ, encapsulate all information about the heat source, base velocity, and ambient conditions. To add the chaotic perturbation of the acoustic velocity at the heat source, and transform the time-delayed problem into a initial value problem, we model the advection of a perturbation v with velocity τ^{-1} as [21]

$$\frac{\partial v}{\partial t} + \frac{1}{\tau}\frac{\partial v}{\partial X} = 0, \quad 0 \le X \le 1, \tag{16}$$

$$v(X = 0, t) = u_f(t). \tag{17}$$

The time-delayed velocity is provided by the value of the dummy variable v at the right boundary, i.e. $u_f(t-\tau)) = v(X = 1, t)$. Physically, (16) represents a generic heat source, in which the time that an acoustic perturbation from the base of the heat source takes to release heat, $\dot{q}$, is τ. More accurate reduced-order models for premixed flames can be found in Waugh et al. [12], Orchini et al. [14], Kashinath et al. [80, 81] and for diffusion flames in Magri and Juniper [41], Tyagi et al. [82].

3.2.1 Chaotic perturbation to the acoustic velocity

The effect of the chaotic hydrodynamics is to perturb the time delay between heat release and velocity perturbations. To model this, the velocity at the base of the heat source is perturbed as

$$v(X = 0, t) = u_f(t) + \alpha x_L, \tag{18}$$

where x_L is the first state variable of the Lorenz system (12), which acts as the chaotic forcing. When $\alpha = 0$, we recover the non-chaotic time-delayed model. Physically, this means that the acoustics do not affect the hydrodynamics. The source of chaos is one-way coupled to the thermoacoustic system, which acts as an additive disturbance to the acoustic velocity (Figure 2). This one-way coupling is physically justified at first order in low-Mach number flows when the acoustics and hydrodynamics have different temporal scales. This can be shown by a multiple-scale method applied to the reacting Navier-Stokes equations, as explained in Section 3.4 of [83].

3.2.2 Numerical discretisation

Equations (13), (14) are discretised by a Galerkin method [84]. First, the acoustic variables are separated in time and space as

$$u(x,t) = \sum_{j=1}^{N_g} \eta_j(t)\cos(j\pi x), \tag{19}$$

$$p(x,t) = -\sum_{j=1}^{N_g} \mu_j(t)\sin(j\pi x), \tag{20}$$

where each spatial function is a natural acoustic mode of the open-ended duct. The partial differential equation (14) is projected onto the Galerkin spatial basis $\{\cos(\pi x), \cos(2\pi x), \ldots, \cos(N_g\pi x)\}$ to yield

$$\dot{\eta}_j - j\pi\mu_j = 0 \tag{21}$$

$$\dot{\mu}_j + j\pi\eta_j + \zeta_j\mu_j + 2\dot{q}\sin(j\pi x_f) = 0. \tag{22}$$

The system has $2N_g$ degrees of freedom. The time-delayed velocity becomes

$$u_f(t-\tau) = \sum_{k=1}^{N_g} \eta_k(t-\tau)\cos(k\pi x_f), \tag{23}$$

and the damping, ζ_j, is modelled by a modal expression that damps out higher-frequency oscillations, $\zeta_j = c_1 j^2 + c_2 j^{1/2}$, where $c_1 = 0.05$ and $c_2 = 0.01$ [42]. This damping model originates from physical principles, as explained in Landau and Lifshitz [85]. We have assumed that the mean flow is sufficiently slow such that it can be neglected. Adding a mean flow may quantitatively change the phases between acoustic waves [86], but the conclusions of this paper are qualitatively unaffected. With a mean flow, a wave-approach can be used instead [86].

The linear advection equation (16) is discretised using $N_c + 1$ points with a Chebyshev spectral method [87]. This discretisation adds N_c degrees of freedom. The resulting discretised system is time-integrated using the 3-stage Runge-Kutta scheme by Wray [88]. On numerical discretisation, the thermoacoustic state vector is $\boldsymbol{q} = \big(\eta_1, \ldots, \eta_{N_g},\ \mu_1, \ldots, \mu_{N_g},\ v_1, \ldots, v_{N_c},\ x_L,\ y_L,\ z_L\big)$.

3.2.3 Effect of numerical discretisation

To investigate the effect of the numerical discretisation, we perform tests on a chaotically perturbed limit cycle (Figure 3). Figure 3a shows the standard deviation of $\eta_j(t)$, $j = 1, \cdots, N_g$, for different values of N_g with fixed $N_c + 1 = 11$. The dominant unstable mode is the first mode because the heat source is located at $x_f = 0.3$, where most of the energy excites the first mode. The calculations with small N_g correctly capture the energy associated with each of the Galerkin modes that they compute. When increasing the number of Galerkin modes, the accuracy on the modes that were previously included does not improve. The benefit of increasing N_g is to increase the spatial resolution by including higher wavenumbers. The magnitude of the standard deviation decays sharply at the beginning up to $j \approx 10$, followed by a slower decay. Therefore, capturing modes of lower intensity requires a large increase in the number of Galerkin modes. We choose $N_g = 10$ as a good compromise between accuracy and computational cost.

4 Stability and hyperbolicity of the chaotically perturbed acoustic limit cycle

In Section 5, the sensitivities of the time-averaged acoustic energy and Rayleigh index with respect to the heat-source parameters are computed in a chaotically perturbed acoustic limit cycle. Subsequently, such sensitivities are embedded into an optimisation routine to suppress a large chaotic oscillation in a bistable region (Section 6). However, as discussed in Section 2, first, we wish to show that the thermoacoustic chaotic attractor is hyperbolic, otherwise the sensitivities of (1) may not exist. The initial condition is $\boldsymbol{q}_0 = [1 \cdots 1]$. The acoustic velocity is

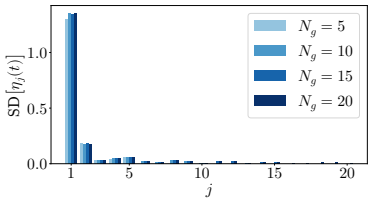

(a) Varying N_g, with fixed $N_c + 1 = 11$.

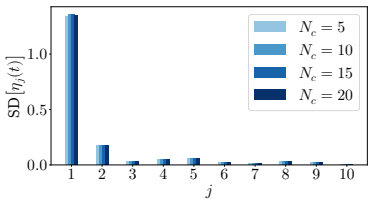

(b) Varying N_c, with fixed $N_g = 10$.

Fig. 3: Convergence study on the standard deviation of the Galerkin modes, $\eta_j(t)$, on a chaotically perturbed acoustic limit cycle ($\alpha = 0.01$). The tenth mode is of the order of machine precision.

chaotically perturbed by setting the coupling parameter to $\alpha = 0.01$ in (18), which corresponds to a chaotic disturbance of approximately 1-10% of the first mode's amplitude. In a chaotic solution, only covariant Lyapunov vector analysis can calculate the linear dynamics of the attractor. Eigenvalue and Floquet analyses are not valid. The acoustic velocity at the base of the heat source, $u_f(t)$, is oscillatory (Figure 4) but aperiodic. The Lyapunov spectrum is shown in Figure 5. The first Lyapunov exponent, $\lambda_1 \approx 0.91038$, is positive, and is close to the positive Lyapunov exponent of the Lorenz system [64] because the chaotic disturbance is one-way coupled to the thermoacoustic system (Figure 2). This means that the Lyapunov exponent of the chaotic perturbation is virtually unaffected when feeding the thermoacoustics, i.e. it acts similarly to a chaotic external forcing. $\boldsymbol{\phi}_2(t)$ is the neutral covariant Lyapunov vector because $\lambda_2 = 0$ to numerical error. Most of the other Lyapunov exponents come in pairs, except for λ_3, λ_4 and λ_{23}, each corresponding to one one-dimensional Lyapunov subspaces. The unstable, neutral and stable subspaces are

$$E^u(t) = \text{Span}[\boldsymbol{\phi}_1(t)] \tag{24}$$
$$E^n(t) = \text{Span}[\boldsymbol{\phi}_2(t)] \tag{25}$$
$$E^s(t) = \text{Span}[\boldsymbol{\phi}_3(t), \cdots, \boldsymbol{\phi}_{33}(t)], \tag{26}$$

respectively. The probability density functions of the angles between the three pairs of elements from E^u, E^n, E^s are shown in Figure 6. In all cases, the probability for a tangency to occur is zero, which shows that the attractor is hyperbolic. However, it must be noted that while no tangencies are present, the minimum observed value

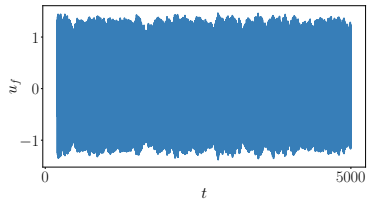

Fig. 4: Acoustic velocity at the heat-source location, $u_f(t)$.

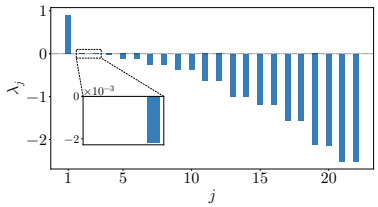

Fig. 5: Lyapunov spectrum (first 22 exponents out of 33). Lyapunov exponents: $\lambda_1 \approx 0.903$, $\lambda_2 \approx -4.2 \times 10^{-5}$ (corresponds to the neutral covariant Lyapunov vector). $\lambda_{23} \approx -14.6$ and Lyapunov exponents of higher index are in the range $[-240, -90]$.

of the angle $\theta_{u,n}$ is 1.2 °, which is very small. As shown by Ni [89], the bound on the error of the non-intrusive least-squares shadowing method is controlled by the minimal angle – the smaller it is, the larger the bound – and an indicative threshold of approximately 5°, which is not verified here, is suggested for accurate results. This issue is tackled with the use of the filtering parameter by Blonigan and Wang [54] and is further developed in Section 5.

In conclusion, the chaotic thermoacoustic system behaves hyperbolically. The nonlinearity of the heat-release response does not change the hyperbolic nature of the chaotic perturbation of the hydrodynamic subsystem. Physically, this means that time-averaged cost functionals of chaotic acoustic oscillations respond smoothly to small changes in the design parameters. This is a key result because it implies that the sensitivities exist. As previously explained, to determine whether a system is hyperbolic, the complete spectrum should be computed to construct the unstable, neutral and stable subspaces. This is possible with the reduced-order model of this paper, but it could be prohibitively expensive in high-dimensional systems, such as large-eddy simulation [4]. For the latter, only a portion of the Lyapunov spectrum and covariant vectors is typically calculated [e.g., 90, 91].

5 Sensitivity and optimisation of chaotic acoustic oscillations

5.1 Time-averaged cost functionals

We analyse the chaotic acoustic oscillation of Section 4. Because thermoacoustics is a multi-physical phenomenon, there are different norms [92, 93], semi-norms [94, 95], and functionals to define a physical measure. For thermoacoustic systems with negligible mean flow, which cannot advect flow inhomogeneities like entropy spots, the acoustic energy and Rayleigh index are two suitable quantities of interest. The instantaneous acoustic energy of the whole system is defined as

$$E_{ac}(t) \triangleq \frac{1}{2}\int_0^1 \left(u^2(t) + p^2(t)\right) dx, \tag{27}$$

which is the sum of the acoustic kinetic and potential energies, i.e., it is the Hamiltonian (constant of motion) of the natural acoustic system. Because of Parseval's theorem, the acoustic energy is related to the Galerkin modes as $E_{ac}(t) = \frac{1}{4}\sum_{j=1}^{N_g}\left(\eta_j^2(t) + \mu_j^2(t)\right)$. The acoustic energy, E_{ac}, is (half) the Euclidean norm of the thermoacoustic system under investigation. In chaotic acoustic oscillations, we

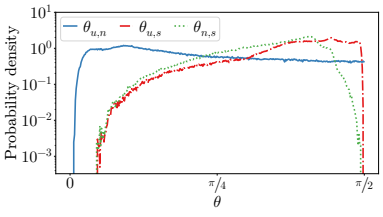

Fig. 6: Probability density function of angles between E^u, E^n, E^s.

are interested in calculating the sensitivity of the time-averaged acoustic energy, $\langle E_{ac} \rangle$.

The Rayleigh index can be derived by (i) multiplying the acoustic momentum equation (13) by u; (ii) multiplying the acoustic energy equation (14) by p; (iii) adding them up; and (iv) integrating in the space domain. This procedure yields an equation for the evolution of the acoustic energy

$$\frac{dE_{ac}}{dt} = -\int_0^1 \zeta p^2 \, dx + p_f \dot{q}, \tag{28}$$

where the Rayleigh index is defined as

$$I_{Ra} \triangleq p_f \dot{q}(t), \tag{29}$$

which, on numerical discretisation, reads

$$I_{Ra} = -\dot{q}\left(v_{N_c}(t)\right) \sum_{j=1}^{N_g} \mu_j(t) \sin(j\pi x_f). \tag{30}$$

The Rayleigh index is a key cost functional that determines the stability of acoustic oscillations fed by a heat source. Physically, (28) states that the acoustic energy grows in time when the pressure at the heat source is sufficiently in phase with the heat release rate to exceed damping mechanisms. The acoustic energy grows up to nonlinear saturation, after which the self-sustained acoustic oscillation persists. This mechanism is commonly referred to as the Rayleigh criterion [6]. In chaotic oscillations, we are interested in calculating the sensitivity of the time-averaged Rayleigh index, $\langle I_{Ra} \rangle$. Applying the infinite time average to (28), and considering that the acoustic energy is a bounded quantity on a strange attractor, yields

$$\begin{aligned} 0 &= \left\langle \frac{dE_{ac}}{dt} \right\rangle + \left\langle \int_0^1 \zeta p^2 \, dx + p_f \dot{q} \right\rangle \\ &= \lim_{T\to\infty} \frac{1}{T} \int_0^T \frac{dE_{ac}}{dt} dt + \left\langle \int_0^1 \zeta p^2 \, dx \right\rangle - \langle p_f \dot{q} \rangle \\ &= \lim_{T\to\infty} \frac{E_{ac}(T) - E_{ac}(0)}{T} + \left\langle \int_0^1 \zeta p^2 \, dx \right\rangle - \langle p_f \dot{q} \rangle , \end{aligned} \tag{31}$$

which physically means that the damping mechanism exactly balances the acoustic source at regime, i.e.,

$$\langle I_{Ra} \rangle \triangleq \langle p_f \dot{q} \rangle = \left\langle \int_0^1 \zeta p^2 \, dx \right\rangle . \tag{32}$$

Thus, the time-averaged Rayleigh index can be expressed either from the heat-source contribution or the dissipation term. From a computational point of view, the calculation of the sensitivity of $\langle p_f \dot{q} \rangle$ is difficult because the chaotic perturbation, which is imposed exactly at $x = x_f$, makes $\langle p_f \dot{q} \rangle$ erratic. To overcome this computational problem, we advise using $\left\langle \int_0^1 \zeta p^2 \, dx \right\rangle$ (bearing in mind the equality (32)), which numerically behaves regularly because it is an integral quantity. Note that the cost functional $\langle I_{Ra} \rangle$ is neither a norm nor a semi-norm. The sensitivity and optimisation framework we propose can tackle general cost functionals.

5.2 Sensitivities

We compute the sensitivities of the time-averaged acoustic energy and Rayleigh index with respect to the heat-source parameters β and τ. Because we have two quantities of interest and two parameters, we use a forward sensitivity method, i.e., an adjoint method would not reduce the number of computations [40, 42, 96]. The nominal parameter values are $\beta_0 = 0.82$ and $\tau_0 = 0.04$. We simplify the notation by representing the finite time-averaged statistics with the same symbol as the infinitely time-averaged ones, $\langle \mathcal{J} \rangle$, since the former are used as a proxy for the latter.

5.2.1 Non-Intrusive Least Squares Shadowing

We apply the Non-Intrusive Least Squares Shadowing (NILSS) over 100000 segments, with a run-up time of 500 time units. Each segment is 200 time steps long (time step of 2×10^{-3} time units), which is between one third and half of the Lyapunov time (see Fig. 5). With the NILSS, the time domain is partitioned in multiple segments, the length of which scales with the Lyapunov time (inverse of the leading Lyapunov exponent).

Figure 7 reports the evolution of $\partial\langle E_{ac}\rangle/\partial\tau$ versus the segment number. The ϵ in the legend refers to the filtering parameter of Blonigan and Wang [54], which we describe here briefly. Part of the NILSS algorithm is the minimisation of the norm of a vector. This is done by solving a linear system $\boldsymbol{S}\boldsymbol{x} = \boldsymbol{b}$, where $\boldsymbol{S}$ is a Schur complement matrix. If a system exhibits tangencies, this matrix becomes rank-deficient and there is no solution to the linear system. In systems that exhibit near-tangencies (small non-zero minimal angle), such as ours (see Fig. 6), the ratio of the largest eigenvalue of $\boldsymbol{S}$ over the smallest becomes very large. In other words, $\boldsymbol{S}$ becomes ill-conditioned. By adding $\epsilon\boldsymbol{I}$ to $\boldsymbol{S}$, where $\boldsymbol{I}$ is the identity matrix, for a range of small ϵ, the smallest eigenvalue becomes approximately equal to ϵ, while the largest is virtually unaffected. Thus, if a large enough ϵ is chosen, the conditioning of the linear problem is improved. Figure 7 shows that the unconditioned ($\epsilon = 0$) NILSS oscillates widely and does not converge in 100000 segments. By making $\epsilon = 10^{-6} \neq 0$, the behaviour is greatly stabilised. However, if ϵ is increased to 10^{-5}, the value of the converged sensitivity is different from that of 10^{-6}. By successively increasing ϵ to 10^{-1}, a trend emerges where the difference of the sensitivities becomes smaller and smaller, implying that the sensitivities approach a limit, which should correspond to the true sensitivity. This is evidence that the use of the NILSS method in systems with small minimal angle can be greatly improved with the use of the filtering parameter. For the remainder of this paper, $\epsilon = 10^{-1}$ is used. The converged values of the sensitivities for the two time-averaged cost functionals, $\langle E_{ac}\rangle$ and $\langle I_{Ra}\rangle$, versus the two parameters, β and τ, are shown in Table 1.

5.2.2 Finite differences

To compute the reference sensitivity solution, we use forward finite differences (first-order) at $\beta = \beta_0(1+\Delta\beta/\beta_0)$ and $\tau = \tau_0(1+\Delta\tau/\tau_0)$, where $\Delta\beta/\beta_0$ and $\Delta\tau/\tau_0$ are varied over $\{10^{-2.5}, 10^{-2}, 10^{-1.5}\}$. The statistics of each point are obtained from an ensemble of 300 simulations of 1000 time units each. At the lower end of the

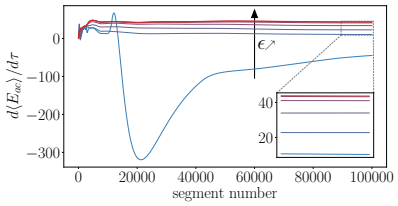

Fig. 7: Evolution of $\partial\langle E_{ac}\rangle/\partial\tau$ versus the number of segments, while varying the filtering parameter, ϵ, in from 10^{-6} to 10^{-1} (red) by steps of one order of magnitude, along with $\epsilon = 0$ (blue). As ϵ is increased, the converged sensitivities tend to a limit, which is the sensitivity of the system.

s	$\partial\langle E_{ac}\rangle/\partial s$	$\partial\langle I_{Ra}\rangle/\partial s$
β	2.34	0.161
τ	43.6	2.78

Table 1: Sensitivities obtained via the NILSS method.

perturbation range, the uncertainty over the cost functional variation is relatively large (Appendix A describes how the uncertainty is calculated). This is due to finite-time averaging error – the smaller the parameter perturbation, the larger the time needed to obtain accurate time averages. Thus, obtaining sensitivities of time averages of unsteady cost functionals via finite differences is computationally expensive and not robust. The chosen range of perturbation values is shown to exhibit a trend close to linear, while its values are relatively large that convergence issues are minimised.

Figure 8 shows the finite difference results with the error bars representing the limits of the interval of confidence (see Appendix A). Notice that a change in sensitivity becomes a vertical shift in these graphs. The shaded region corresponds to values within the uncertainty bounds, such that any line inside it can explain the results of the finite differences under the calculated uncertainty. This region is capped at the top by the largest possible sensitivity. The closer a line is to the points, the better it explains the variations of the time-averaged cost functionals. The red lines, which correspond to the sensitivities calculated with the NILSS method, fit the points well. This verifies that the NILSS method can accurately calculate the sensitivities of time-averaged cost functionals in a chaotic thermoacoustic system.

6 Suppression of a large chaotic acoustic oscillation by optimal design

The thermoacoustic model under investigation displays a bistable region, also known as hysteresis, with a co-existing stable fixed point and a limit cycle, i.e., the Hopf bifurcation is subcritical. Subcritical bifurcations, which are common in thermoacoustic systems [12, 14, 21, 97, 98, 99], are more challenging to control than supercritical bifurcations. On the one hand, ensuring linear stability is nec-

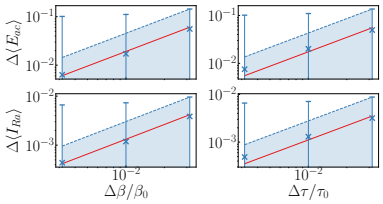

Fig. 8: Comparison between sensitivities obtained by finite differences (blue crosses) and NILSS (red line).

essary and sufficient in supercritical bifurcations: if the system has no unstable eigenvalue, no large self-sustained acoustic oscillation can appear. On the other hand, ensuring linear stability is only necessary in subcritical bifurcations: the system may have large self-sustained acoustic oscillations in the bistable region, where all eigenvalues are stable. Such a situation occurs in the bistable region, where the large self-sustained oscillation may be triggered by a sufficiently large perturbation to the state vector. Nonlinear optimisation has to be employed in the bistable region to find a set of design parameters for which the system is stable to all perturbations. The objective of industry is to operate in the linearly stable region outside the bistable region. In other words, we want to provide a method to answer the question: What is the minimal change of design parameters for which no large oscillation? The answer is provided by either calculating the bifurcation diagram in the multidimensional parameter space, which is computationally cumbersome, or by solving a constrained nonlinear optimisation problem of a time-averaged cost functional, which is computationally affordable. Following the latter route, the optimisation problem is formulated as

$$\begin{aligned} &\underset{\beta,\tau}{\text{minimise}} \quad \langle \mathcal{J}(\beta,\tau)\rangle \\ &\text{subject to} \quad (13),(14),(15),(16),(19),(20) \end{aligned} \tag{33}$$

where $\mathcal{J}$ is either the acoustic energy (27), E_{ac}, or the Rayleigh index (32), I_{Ra}. The set of parameters can be updated by a steepest descent method

$$\boldsymbol{s}_{n+1} = \boldsymbol{s}_n - \gamma \nabla_{\boldsymbol{s}} \langle \mathcal{J}\rangle|_{\boldsymbol{s}=\boldsymbol{s}_n}\,, \tag{34}$$

where $\boldsymbol{s} = [\tilde{\beta} \quad \tilde{\tau}]^T$. The normalised parameters vector and the relaxation factor, γ, enable stable and accurate numerical convergence. The normalisation is such that $\beta = \tilde{\beta}\beta_0$ and $\tau = \tilde{\tau}\tau_0$, where β_0 and τ_0 are the starting points of the optimisation. The normalisation makes the orders of magnitude of both parameters the same, which enables robust optimisation despite the gradients in τ being one order of magnitude higher than gradients in β. The relaxation factor γ is 0.01 for the optimisation on the acoustic energy, $\langle E_{ac}\rangle$, and 0.2 for the optimisation on the Rayleigh index, $\langle I_{Ra}\rangle$. The algorithm stops when the condition

$$\langle \mathcal{J}(\beta,\tau)\rangle < \epsilon \cdot \langle \mathcal{J}(\beta_0,\tau_0)\rangle \tag{35}$$

is met, where $\epsilon = 5\%$. This condition physically signifies that the optimisation is successful when the thermoacoustic system vibrates around the fixed point, with

the energy content being related to the chaotic perturbation of the hydrodynamic field only. The sensitivities are calculated with the NILSS method over 20000 segments, each of 200 time steps (time step of 2×10^{-3} time units), a run-up time of a 1000 time units and the filtering parameter is set to 10^{-1}.

Figures 9a and 9b show the suppression of the chaotically perturbed acoustic limit cycle by optimally changing the heat-source parameters. The stopping condition (35) is satisfied after 3 (acoustic energy) or 2 (Rayleigh index) iterations and an extra iteration is performed to ensure that the time-averaged cost functional does not change. This routine can be used to accurately detect the fold point by reducing the relaxation factor, γ, at the cost of more iterations. An optimisation using sensitivities of the eigenvalues at the fixed point would have stopped at the initial design point, (β_0, τ_0), because all the eigenvalues would be stable (located in the bistable region). However, because we used the sensitivities of the chaotically perturbed acoustic limit cycle, we were able to stabilise the chaotically perturbed thermoacoustic limit cycle to all perturbations.

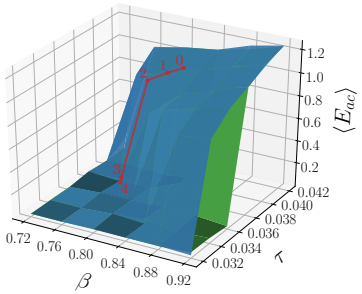

(a) Optimisation of the time-averaged acoustic energy.

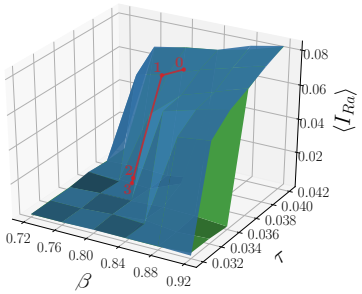

(b) Optimisation of the time-averaged Rayleigh index.

Fig. 9: Suppression of a chaotic acoustic oscillation in the bistable region. The optimisation route is overlayed (red line) on top of the upper branch (blue) and the lower branch (green). The labels correspond to the optimisation step. The optimisation starts at $\beta_0 = 0.82$, $\tau_0 = 0.04$, where two attractors co-exist: a chaotic attractor around the fixed point, $\bar{\boldsymbol{q}} = 0$, and a chaotically perturbed acoustic limit cycle.

7 Conclusions

The preliminary design of thermoacoustic systems is traditionally based on eigenvalue analysis [5, 40]. Recent developments in eigenvalue sensitivity methods [40] have enabled gradient-based optimisation of thermoacoustic systems. These methods allowed the optimal design parameters to be computed to ensure that the system operates in a linearly stable region [46, 47]. Linear stability, however, cannot guarantee that a nonlinear thermoacoustic oscillation will not occur. This is the case of subcritical bifurcations, in which a large-amplitude thermoacoustic *limit cycle* can be triggered from a linearly stable solution. To complicate the picture, realistic combustors operate in a turbulent environment. The action of turbulence in a thermoacoustic oscillation is that of chaotically perturbing the limit cycle. Consequently, high-fidelity-simulation-driven optimal design calls for nonlinear tools that are able to tackle chaotic systems. In this paper, we propose a framework to optimise a chaotically perturbed limit cycle. The effect of turbulence is *qualitatively* modelled as a chaotic perturbation to the heat released by a source.

Covariant Lyapunov vector analysis is employed to calculate the sensitivity of the chaotic thermoacoustic solutions. We show that the nonlinear heat-release response does not change the hyperbolic nature of the chaotic perturbation. The chaotically perturbed thermoacoustic system is hyperbolic, thus, time-averaged thermoacoustic cost functionals respond smoothly to small changes to the design parameters. By exploiting hyperbolicity, we apply the non-intrusive least-squares shadowing method [53] to calculate the sensitivities of the time-averaged acoustic energy and Rayleigh index, which are two key cost functionals used in thermoacoustics. The sensitivities are employed as gradients in an optimisation routine to suppress a chaotically perturbed acoustic limit cycle by changing the heat-source parameters. This result cannot be achieved by only stabilising the eigenvalues, nor can it be achieved by traditional sensitivity methods that work in non-chaotic oscillations. This work opens up new possibilities for the control of unsteady acoustic oscillations in turbulent combustors. The method proposed can be used with virtually no conceptual modification in unsteady high-fidelity simulations with the aid of high-performance computing. Because the theoretical framework is based on dynamical systems theory, the techniques presented can be used in other unsteady *deterministic multi-physics* problems.

Acknowledgments

F. Huhn is supported by Fundação para a Ciência e Tecnologia in Portugal under the Research Studentship No. SFRH/BD/134617/2017. L. Magri gratefully acknowledges financial support from the Royal Academy of Engineering Research Fellowships. Fruitful discussions with Prof. Q. Wang, Dr. P. Blonigan, N. Chandramoorthy and A. Ni are gratefully acknowledged. We are grateful to Dr. Patrick Blonigan for his insightful suggestions on using the filtering parameter.

Conflict of Interest: The authors declare that they have no conflict of interest.

A Uncertainty on the estimation of infinitely time-averaged cost functionals

We wish to estimate the value of an infinitely time-averaged cost functional, $\langle \mathcal{J} \rangle$, from a collection of N independent samples of the time-averaged cost functional, $\{\langle \mathcal{J} \rangle_T^{(i)}\}$, where the subscript T and superscript (i) represent the finite time used in the averaging and the index of the sample, respectively. From the Central Limit Theorem, we assume that the error in the estimation of $\langle \mathcal{J} \rangle$ decays with the number of samples used to the power of $-1/2$. Thus, we set a nonlinear constrained minimisation problem

$$\begin{aligned} &\underset{a,b}{\text{minimise}} \quad b \\ &\text{subject to} \quad a - \frac{b}{\sqrt{n}} < \frac{1}{n}\sum_{i=1}^{n} \langle \mathcal{J} \rangle_T^{(i)} < a + \frac{b}{\sqrt{n}}. \\ &\qquad\qquad\qquad\qquad \forall\, n \in \{1, \cdots, N\} \end{aligned} \tag{36}$$

Thus, $\langle \mathcal{J} \rangle$ should be in the range $\left(a - b/\sqrt{N}, a + b/\sqrt{N}\right)$.

References

1. T. C.Lieuwen and V.Yang. *Combustion Instabilities in Gas Turbine Engines: Operational Experience, Fundamental Mechanisms, and Modeling*. American Institute of Aeronautics and Astronautics, Inc., 2005. ISBN 156347669X. URL `http://www.lavoisier.fr/livre/notice.asp?id=RAXW2KALXX6OWV`.
2. F. E. C.Culick. *Unsteady motions in combustion chambers for propulsion systems*. RTO AGARDograph AG-AVT-039, North Atlantic Treaty Organization, 2006. ISBN 9789283700593.
3. A. P.Dowling and Y.Mahmoudi. Combustion noise. *Proceedings of the Combustion Institute*, 35(1):65–100, 2015. ISSN 15407489. doi: 10.1016/j.proci.2014.08.016. URL `http://dx.doi.org/10.1016/j.proci.2014.08.016`.
4. T.Poinsot. Prediction and control of combustion instabilities in real engines. *Proceedings of the Combustion Institute*, 36(1):1–28, 2017. ISSN 15407489. doi: 10.1016/j.proci.2016.05.007. URL `http://linkinghub.elsevier.com/retrieve/pii/S1540748916300074`.
5. M. P.Juniper and R. I.Sujith. Sensitivity and nonlinearity of thermocoustic oscillations. *Annual Review of Fluid Mechanics*, 50(1):661–689, 2018. doi: 10.1146/annurev-fluid-122316-045125. URL `https://doi.org/10.1146/annurev-fluid-122316-045125`.
6. L.Rayleigh. The explanation of certain acoustical phenomena. *Nature*, 18:319 –, 1878. ISSN 1540-7489. doi: http://dx.doi.org/10.1038/018319a0.
7. L.Kabiraj, R. I.Sujith, and P.Wahi. Bifurcations of Self-Excited Ducted Laminar Premixed Flames. *Journal of Engineering for Gas Turbines and Power*, 134(3):31502, 2011. ISSN 0742-4795. doi: 10.1115/1.4004402. URL `http://dx.doi.org/10.1115/1.4004402`.
8. H.Gotoda, H.Nikimoto, T.Miyano, and S.Tachibana. Dynamic properties of combustion instability in a lean premixed gas-turbine combustor. *Chaos*, 21(1):013124, mar 2011. ISSN 1089-7682. doi: 10.1063/1.3563577. URL `http://www.ncbi.nlm.nih.gov/pubmed/21456838`.
9. H.Gotoda, T.Ikawa, K.Maki, and T.Miyano. Short-term prediction of dynamical behavior of flame front instability induced by radiative heat loss. *Chaos*, 22(1):033106, sep 2012. ISSN 1089-7682. doi: 10.1063/1.4731267. URL `http://www.ncbi.nlm.nih.gov/pubmed/23020445`.
10. L.Kabiraj, A.Saurabh, P.Wahi, and R. I.Sujith. Route to chaos for combustion instability in ducted laminar premixed flames. *Chaos*, 22(2):0–12, 2012. ISSN 10541500. doi: 10.1063/1.4718725.
11. K.Kashinath, I. C.Waugh, and M. P.Juniper. Nonlinear self-excited thermoacoustic oscillations of a ducted premixed flame: bifurcations and routes to chaos. *Journal of Fluid Mechanics*, 761:399–430, 2014. ISSN 0022-1120. doi: 10.1017/jfm.2014.601. URL `http://www.journals.cambridge.org/abstract_S0022112014006016`.

12. I. C.Waugh, K.Kashinath, and M. P.Juniper. Matrix-free continuation of limit cycles and their bifurcations for a ducted premixed flame. *Journal of Fluid Mechanics*, 759: 1–27, 2014. ISSN 0022-1120. doi: 10.1017/jfm.2014.549. URL http://www.journals.cambridge.org/abstract_S0022112014005497.
13. V.Nair, G.Thampi, and R. I.Sujith. Intermittency route to thermoacoustic instability in turbulent combustors. *Journal of Fluid Mechanics*, 756:470–487, 2014. ISSN 1469-7645. doi: 10.1017/jfm.2014.468.
14. a.Orchini, S. J.Illingworth, and M. P.Juniper. Frequency domain and time domain analysis of thermoacoustic oscillations with wave-based acoustics. *Journal of Fluid Mechanics*, 775: 387–414, 2015. ISSN 0022-1120. doi: 10.1017/jfm.2015.139. URL http://www.journals.cambridge.org/abstract_S0022112015001391.
15. V.Nair and R. I.Sujith. A reduced-order model for the onset of combustion instability: Physical mechanisms for intermittency and precursors. *Proceedings of the Combustion Institute, in press*, 35(3):3193–3200, jul 2015. ISSN 15407489. doi: 10.1016/j.proci.2014.07.007. URL http://linkinghub.elsevier.com/retrieve/pii/S1540748914003174.
16. A. P.Dowling. Nonlinear self-excited oscillations of a ducted flame. *Journal of Fluid Mechanics*, 346:271–290, 1997. doi: 10.1017/S0022112097006484. URL http://www.journals.cambridge.org/abstract_S0022112097006484.
17. A. P.Dowling. A kinematic model of a ducted flame. *Journal of Fluid Mechanics*, 394: 51–72, 1999. doi: 10.1017/S0022112099005686. URL http://www.journals.cambridge.org/abstract_S0022112099005686.
18. J.-P.Eckmann. Roads to turbulence in dissipative dynamical systems. *Reviews of Modern Physics*, 53(4):643–654, 1981.
19. J.Miles. Strange attractors in fluid dynamics. *Advances in Applied Mechanics*, 24:189–214, 1984.
20. J. P.Eckmann and D.Ruelle. Ergodic theory of chaos and strange attractors. *Reviews of Modern Physics*, 57:617–656, 1985. ISSN 00346861. doi: 10.1103/RevModPhys.57.617.
21. F.Huhn and L.Magri. Stability, sensitivity and optimisation of chaotic acoustic oscillations. *Journal of Fluid Mechanics*, 882:A24, 2020. doi: 10.1017/jfm.2019.828. URL http://arxiv.org/abs/1909.12979.
22. T.Lieuwen. *Unsteady Combustor Physics*. Cambridge University Press, 2012.
23. N.Noiray and B.Schuermans. Deterministic quantities characterizing noise driven Hopf bifurcations in gas turbine combustors. *International Journal of Non-Linear Mechanics*, 50:152–163, 2013. ISSN 00207462. doi: 10.1016/j.ijnonlinmec.2012.11.008. URL http://dx.doi.org/10.1016/j.ijnonlinmec.2012.11.008.
24. N.Noiray. Linear Growth Rate Estimation from Dynamics and Statistics of Acoustic Signal Envelope in Turbulent Combustors. *Journal of Engineering for Gas Turbines and Power*, 139(4):041503, 2016. doi: 10.1115/1.4034601.
25. N.Noiray and A.Denisov. A method to identify thermoacoustic growth rates in combustion chambers from dynamic pressure time series. *Proceedings of the Combustion Institute*, 36(3):3843–3850, 2017. ISSN 15407489. doi: 10.1016/j.proci.2016.06.092. URL http://dx.doi.org/10.1016/j.proci.2016.06.092.
26. K. I.Matveev and F. E. C.Culick. A model for combustion instability involving vortex shedding. *Combustion Science and Technology*, 175:1059–1083, 2003. URL http://www.tandfonline.com/doi/abs/10.1080/00102200302349.
27. P.Duncan Thompson. Uncertainty of Initial State as a Factor in the Predictability of Large Scale Atmospheric Flow Patterns. *Tellus A*, 9:275–295, 1957. ISSN 0280-6495. doi: 10.3402/tellusa.v9i3.9111.
28. R. G.Deissler. Is Navier–Stokes turbulence chaotic? *Physics of Fluids*, 29(5):1453, jun 1986. ISSN 00319171. doi: 10.1063/1.865663. URL https://aip.scitation.org/doi/10.1063/1.865663.
29. G.Boffetta, M.Cencini, M.Falcioni, and A.Vulpiani. Predictability: a way to characterize complexity. *Physics Reports*, 356:367–474, 2002. ISSN 0370-1573. doi: 10.1016/S0370-1573(01)00025-4.
30. G.Nastac, J.Labahn, L.Magri, and M.Ihme. Lyapunov exponent as a metric for assessing the dynamic content and predictability of large-eddy simulations. *Physical Review Fluids*, 2(9):094606, 2017. ISSN 2469990X. doi: 10.1103/PhysRevFluids.2.094606.
31. E. N.Lorenz. Deterministic nonperiodic flow. *Journal of the Atmospheric Sciences*, 20 (2):130–141, 1963. doi: 10.1175/1520-0469(1963)020⟨0130:DNF⟩2.0.CO;2. URL https://doi.org/10.1175/1520-0469(1963)020<0130:DNF>2.0.CO;2.

32. L.Selle, R.Blouquin, M.Théron, L. H.Dorey, M.Schmid, and W.Anderson. Prediction and analysis of combustion instabilities in a model rocket engine. *Journal of Propulsion and Power*, 30(4):978–990, 2014. ISSN 07484658. doi: 10.2514/1.B35146.
33. A.Ghani, T.Poinsot, L.Gicquel, and J. D.Müller. LES Study of Transverse Acoustic Instabilities in a Swirled Kerosene/Air Combustion Chamber. *Flow, Turbulence and Combustion*, 96(1):207–226, 2016. ISSN 15731987. doi: 10.1007/s10494-015-9654-9.
34. J. O.Brien, J.Kim, and M.Ihme. Investigation of the mechanisms of jet-engine core noise using large-eddy simulation. *AIAA 54th Aerospace Sciences Meeting*, pages 2016–0761, 2016. doi: 10.2514/6.2016-0761.
35. H.Gotoda, Y.Okuno, K.Hayashi, and S.Tachibana. Characterization of degeneration process in combustion instability based on dynamical systems theory. *Physical Review E - Statistical, Nonlinear, and Soft Matter Physics*, 92(5):1–11, 2015. ISSN 15502376. doi: 10.1103/PhysRevE.92.052906.
36. V. R.Unni and R. I.Sujith. Multifractal characteristics of combustor dynamics close to lean blowout. *Journal of Fluid Mechanics*, 784:30–50, 2015. ISSN 0022-1120. doi: 10.1017/jfm.2015.567. URL `http://www.journals.cambridge.org/abstract_S0022112015005674`.
37. M.Murugesan and R. I.Sujith. Combustion noise is scale-free: transition from scale-free to order at the onset of thermoacoustic instability. *Journal of Fluid Mechanics*, 772: 225–245, 2015. ISSN 0022-1120. doi: 10.1017/jfm.2015.215. URL `http://www.journals.cambridge.org/abstract_S0022112015002153`.
38. S. A.Pawar, A.Seshadri, V. R.Unni, and R. I.Sujith. Thermoacoustic instability as mutual synchronization between the acoustic field of the confinement and turbulent reactive flow. *Journal of Fluid Mechanics*, 827:664–693, 2017. ISSN 14697645. doi: 10.1017/jfm.2017.438.
39. S.Mondal, V. R.Unni, and R. I.Sujith. Onset of thermoacoustic instability in turbulent combustors: An emergence of synchronized periodicity through formation of chimera-like states. *Journal of Fluid Mechanics*, 811:659–681, 2017. ISSN 14697645. doi: 10.1017/jfm.2016.770.
40. L.Magri. Adjoint methods as design tools in thermoacoustics. *Applied Mechanics Reviews*, 71, 2019. doi: http://dx.doi.org/10.1115/1.4042821.
41. L.Magri and M. P.Juniper. Global modes, receptivity, and sensitivity analysis of diffusion flames coupled with duct acoustics. *Journal of Fluid Mechanics*, 752:237–265, 2014. doi: 10.1017/jfm.2014.328.
42. L.Magri and M. P.Juniper. Sensitivity analysis of a time-delayed thermo-acoustic system via an adjoint-based approach. *Journal of Fluid Mechanics*, 719:183–202, 2013. doi: 10.1017/jfm.2012.639.
43. L.Magri, M.Bauerheim, F.Nicoud, and M. P.Juniper. Stability analysis of thermo-acoustic nonlinear eigenproblems in annular combustors. Part II. Uncertainty quantification. *Journal of Computational Physics*, 325:411–421, 2016. ISSN 10902716. doi: 10.1016/j.jcp.2016.08.043. URL `http://dx.doi.org/10.1016/j.jcp.2016.08.043`.
44. C. F.Silva, L.Magri, T.Runte, and W.Polifke. Uncertainty Quantification of Growth Rates of Thermoacoustic Instability by an Adjoint Helmholtz Solver. *Journal of Engineering for Gas Turbines and Power*, 139(1):011901, 2016. ISSN 0742-4795. doi: 10.1115/1.4034203. URL `http://gasturbinespower.asmedigitalcollection.asme.org/article.aspx?doi=10.1115/1.4034203`.
45. G. A.Mensah, L.Magri, and J. P.Moeck. Methods for the calculation of thermoacoustic stability margins and Monte-Carlo free uncertainty quantification. *Journal of Engineering for Gas Turbines and Power*, 140(6):061501, 2018. doi: 10.1115/1.4038156.
46. G. A.Mensah and J. P.Moeck. Acoustic Damper Placement and Tuning for Annular Combustors: An Adjoint-Based Optimization Study. *Journal of Engineering for Gas Turbines and Power*, 139(6):061501, 2017. ISSN 0742-4795. doi: 10.1115/1.4035201. URL `http://gasturbinespower.asmedigitalcollection.asme.org/article.aspx?doi=10.1115/1.4035201`.
47. J.Aguilar and M. P.Juniper. Adjoint methods for elimination of thermoacoustic oscillations in a model annular combustor via small geometry modifications. In *ASME Turbo Expo, Oslo, Norway*, pages GT2018–75692, 2018.
48. G. D.Birkhoff. Proof of the ergodic theorem. *Proceedings of the National Academy of Sciences of the United States of America*, 17(12):656–660, 1931.
49. D. J.Lea, M. R.Allen, and T. W.Haine. Sensitivity analysis of the climate of a chaotic system. *Tellus A: Dynamic Meteorology and Oceanography*, 52(5):523–532, 2000. doi:

10.3402/tellusa.v52i5.12283. URL https://doi.org/10.3402/tellusa.v52i5.12283.
50. G. L.Eyink, T. W.Haine, and D. J.Lea. Ruelle's linear response formula, ensemble adjoint schemes and Lévy flights. *Nonlinearity*, 17(5):1867–1889, 2004. ISSN 09517715. doi: 10.1088/0951-7715/17/5/016.
51. Q.Wang. Forward and adjoint sensitivity computation of chaotic dynamical systems. *Journal of Computational Physics*, 235:1 – 13, 2013. ISSN 0021-9991. doi: https://doi.org/10.1016/j.jcp.2012.09.007. URL http://www.sciencedirect.com/science/article/pii/S0021999112005360.
52. Q.Wang, R.Hu, and P.Blonigan. Least squares shadowing sensitivity analysis of chaotic limit cycle oscillations. *Journal of Computational Physics*, 267:210 – 224, 2014. ISSN 0021-9991. doi: https://doi.org/10.1016/j.jcp.2014.03.002. URL http://www.sciencedirect.com/science/article/pii/S0021999114001715.
53. A.Ni and Q.Wang. Sensitivity analysis on chaotic dynamical systems by non-intrusive least squares shadowing (nilss). *Journal of Computational Physics*, 347:56 – 77, 2017. ISSN 0021-9991. doi: https://doi.org/10.1016/j.jcp.2017.06.033. URL http://www.sciencedirect.com/science/article/pii/S0021999117304783.
54. P. J.Blonigan and Q.Wang. Multiple shooting shadowing for sensitivity analysis of chaotic dynamical systems. *Journal of Computational Physics*, 354:447 – 475, 2018. ISSN 0021-9991. doi: https://doi.org/10.1016/j.jcp.2017.10.032. URL http://www.sciencedirect.com/science/article/pii/S002199911730791X.
55. A.Katok and B.Hasselblatt. *Introduction to the Modern Theory of Dynamical Systems*. Cambridge University Press, 1995.
56. P.Holmes, J. L.Lumley, and G.Berkooz. *Turbulence, Coherent Structures, Dynamical Systems and Symmetry*. Cambridge Monographs on Mechanics. Cambridge University Press, 1996. doi: 10.1017/CBO9780511622700.
57. S. Y.Pilyugin. *Shadowing in dynamical systems*. Springer, 2006.
58. D.Ruelle. A review of linear response theory for general differentiable dynamical systems. *Nonlinearity*, 22(4):855, 2009. URL http://stacks.iop.org/0951-7715/22/i=4/a=009.
59. F.Ginelli, P.Poggi, A.Turchi, H.Chaté, R.Livi, and A.Politi. Characterizing dynamics with covariant lyapunov vectors. *Physical Review Letters*, 99(13):130601, 2007. ISSN 00319007. doi: 10.1103/PhysRevLett.99.130601.
60. F.Ginelli, H.Chaté, R.Livi, and A.Politi. Covariant lyapunov vectors. *Journal of Physics A: Mathematical and Theoretical*, 46(25):254005, 2013. URL http://stacks.iop.org/1751-8121/46/i=25/a=254005.
61. K. A.Takeuchi, H.-l.Yang, F.Ginelli, G.Radons, and H.Chaté. Hyperbolic decoupling of tangent space and effective dimension of dissipative systems. *Phys. Rev. E*, 84:046214, Oct 2011. doi: 10.1103/PhysRevE.84.046214. URL https://link.aps.org/doi/10.1103/PhysRevE.84.046214.
62. V. I.Oseledets. A multiplicative ergodic theorem: Lyapunov characteristic numbers for dynamical systems. *Trans. Moscow Math. Soc.*, 19:197–231, 1968.
63. D.Veynante and L.Vervisch. Turbulent combustion modeling. *Progress in Energy and Combustion Science*, 28:193–266, mar 2002. ISSN 03601285. doi: 10.1016/S0360-1285(01)00017-X. URL http://linkinghub.elsevier.com/retrieve/pii/S036012850100017X.
64. J.Frøyland and K. H.Alfsen. Lyapunov-exponent spectra for the Lorenz model. *Phys. Rev. A*, 29(5):2928–2931, may 1984. doi: 10.1103/PhysRevA.29.2928. URL https://link.aps.org/doi/10.1103/PhysRevA.29.2928.
65. V.Araujo and M. J.Pacifico. *Three-dimensional flows*. A Series of Modern Surveys in Mathematics, Volume 53. Springer, New York, 2010. ISBN 9783642263804.
66. V.Araujo, S.Galatolo, and M. J.Pacifico. Statistical properties of Lorenz like flows, recent developments and perspectives. *International Journal of Bifurcation and Chaos*, 24(10):1430028–1–1430028–34, 2014. doi: 10.1142/S0218127414300286. URL http://arxiv.org/abs/math/0403273%0Ahttp://dx.doi.org/10.1142/S0218127414300286.
67. C.Sparrow. *The Lorenz Equations: Bifurcations, Chaos, and Strange Attractors*. Applied Mathematical Sciences 41. Springer-Verlag New York, 1 edition, 1982. ISBN 978-1-4612-5767-7. doi: 10.1007/978-1-4612-5767-7.
68. G.Gallavotti and E. G. D.Cohen. Dynamical ensembles in stationary states. *Journal of Statistical Physics*, 80(5-6):931–970, sep 1995. ISSN 0022-4715. doi: 10.1007/BF02179860. URL http://link.springer.com/10.1007/BF02179860.
69. G.Gallavotti. Entropy, thermostats, and chaotic hypothesis. *Chaos: An Interdisciplinary Journal of Nonlinear Science*, 16(4):043114, dec 2006. ISSN 1054-1500. doi: 10.1063/1.

2372713. URL http://aip.scitation.org/doi/10.1063/1.2372713.
70. D.Ruelle. Measures Describing a Turbulent Flow. *Annals of the New York Academy of Sciences*, 357(1):1–9, 1980. ISSN 17496632. doi: 10.1111/j.1749-6632.1980.tb29669.x.
71. Y.Pomeau and P.Manneville. Intermittent transition to turbulence in dissipative dynamical systems. *Communications in Mathematical Physics*, 74(2):189–197, 1980. ISSN 00103616. doi: 10.1007/BF01197757.
72. E.Aurell, G.Boffetta, A.Crisanti, G.Paladin, and A.Vulpiani. Growth of non-infinitesimal perturbations in turbulence. *Physical review letters*, 77(7):1262–1265, 1996. ISSN 1079-7114. doi: 10.1103/PhysRevLett.77.1262. URL http://journals.aps.org/prl/abstract/10.1103/PhysRevLett.77.1262%5Cnhttp://arxiv.org/abs/chao-dyn/9604007.
73. K.Balasubramanian and R. I.Sujith. Thermoacoustic instability in a Rijke tube: Non-normality and nonlinearity. *Physics of Fluids*, 20(4):044103, 2008. ISSN 10706631. doi: 10.1063/1.2895634.
74. M. P.Juniper. Triggering in the horizontal rijke tube: non-normality, transient growth and bypass transition. *Journal of Fluid Mechanics*, 667:272–308, 2011. doi: 10.1017/S0022112010004453.
75. L. V.King. On the convection of heat from small cyclinders in a stream of fluid: determination of the convection constants of small platinum wires with applications to hot-wire anemometry. *Proceedings of the Royal Society of ...*, 214(8):373–434, 1914. URL http://rspa.royalsocietypublishing.org/content/90/622/563.full.pdf.
76. M. A.Heckl. Active control of the noise from a Rijke tube. *Journal of Sound and Vibration*, 124(1):117–133, 1988. doi: 10.1016/S0022-460X(88)81408-1. URL http://linkinghub.elsevier.com/retrieve/pii/S0022460X88814081.
77. M. A.Heckl. Non-linear acoustic effects in the Rijke tube. *Acustica*, 72:63–71, 1990. URL http://www.ingentaconnect.com/content/dav/aaua/1990/00000072/00000001/art00010.
78. W.Polifke, A.Poncet, C. O.Paschereit, and K.Döbbeling. Reconstruction of Acoustic Transfer Matrices by Instationary Computational Fluid Dynamics. *Journal of Sound and Vibration*, 245(3):483–510, 2001. ISSN 0022460X. doi: 10.1006/jsvi.2001.3594.
79. A.Orchini, G.Rigas, and M. P.Juniper. Weakly nonlinear analysis of thermoacoustic bifurcations in the rijke tube. *Journal of Fluid Mechanics*, 805:523–550, 2016. doi: 10.1017/jfm.2016.585.
80. K.Kashinath, S.Hemchandra, and M. P.Juniper. Nonlinear Phenomena in Thermoacoustic Systems With Premixed Flames. *Journal of Engineering for Gas Turbines and Power*, 135(6):061502, 2013. ISSN 0742-4795. doi: 10.1115/1.4023305. URL http://gasturbinespower.asmedigitalcollection.asme.org/article.aspx?doi=10.1115/1.4023305.
81. K.Kashinath, S.Hemchandra, and M. P.Juniper. Nonlinear thermoacoustics of ducted premixed flames: The influence of perturbation convection speed. *Combustion and Flame*, 160(12):2856–2865, 2013. ISSN 00102180. doi: 10.1016/j.combustflame.2013.06.019. URL http://dx.doi.org/10.1016/j.combustflame.2013.06.019.
82. M.Tyagi, N.Jamadar, and S.Chakravarthy. Oscillatory response of an idealized two-dimensional diffusion flame: Analytical and numerical study. *Combustion and Flame*, 149 (3):271–285, 2007. doi: 10.1016/j.combustflame.2006.12.020. URL http://linkinghub.elsevier.com/retrieve/pii/S0010218007000284.
83. L.Magri, Y.-C.See, O.Tammisola, M.Ihme, and M.Juniper. Multiple-scale thermo-acoustic stability analysis of a coaxial jet combustor. *Proceedings of the Combustion Institute*, 36 (3), 2017. ISSN 15407489. doi: 10.1016/j.proci.2016.06.009.
84. B. T.Zinn and M. E.Lores. Application of the Galerkin Method in the Solution of Non-linear Axial Combustion Instability Problems in Liquid Rockets. *Combustion Science and Technology*, 4(1):269–278, 1971. ISSN 0010-2202. doi: 10.1080/00102207108952493.
85. L. D.Landau and E. M.Lifshitz. *Fluid Mechanics*. Pergamon Press, second edition, 1987.
86. A. P.Dowling and A. S.Morgans. Feedback Control of Combustion Oscillations. *Annual Review of Fluid Mechanics*, 37:151–182, 2005. doi: 10.1146/annurev.fluid.36.050802.122038. URL http://www.annualreviews.org/doi/abs/10.1146/annurev.fluid.36.050802.122038.
87. L. N.Trefethen. *Spectral methods in MATLAB*, volume 10. Siam, 2000.
88. C. A.Kennedy, M. H.Carpenter, and R.Lewis. Low-storage, explicit runge–kutta schemes for the compressible navier–stokes equations. *Applied Numerical Mathematics*, 35(3):177 – 219, 2000. ISSN 0168-9274. doi: https://doi.org/10.1016/S0168-9274(99)00141-5. URL

http://www.sciencedirect.com/science/article/pii/S0168927499001415.
89. A.Ni. Hyperbolicity, shadowing directions and sensitivity analysis of a turbulent three-dimensional flow. *Journal of Fluid Mechanics*, 863:644–669, 2019. doi: 10.1017/jfm.2018.986.
90. P. J.Blonigan, P.Fernandez, S. M.Murman, Q.Wang, G.Rigas, and L.Magri. Towards a chaotic adjoint for LES. In *Center for Turbulence Research, Summer Program*, 2016.
91. P.Fernandez and Q.Wang. Lyapunov spectrum of the separated flow around the NACA 0012 airfoil and its dependence on numerical discretization. *Journal of Computational Physics*, 350:453–469, 2017. ISSN 10902716. doi: 10.1016/j.jcp.2017.08.056. URL http://dx.doi.org/10.1016/j.jcp.2017.08.056.
92. B. T.Chu. On the Energy Transfer to Small Disturbances in Fluid Flow (Part I). *Acta Mechanica*, 1(3):215–234, 1965.
93. K. J.George and R.Sujith. Disturbance energy norms: A critical analysis. *Journal of Sound and Vibration*, 331(7):1552–1566, mar 2012. ISSN 0022460X. doi: 10.1016/j.jsv.2011.11.027. URL http://linkinghub.elsevier.com/retrieve/pii/S0022460X11009059.
94. L.Magri. *Adjoint methods in thermo-acoustic and combustion instability*. PhD thesis, University of Cambridge, 2015.
95. R. S.Blumenthal, A. K.Tangirala, R.Sujith, and W.Polifke. A systems perspective on non-normality in low-order thermoacoustic models: Full norms, semi-norms and transient growth. *International Journal of Spray and Combustion Dynamics*, 9(1):19–43, 2016. ISSN 1756-8277. doi: 10.1177/1756827716652474. URL http://scd.sagepub.com/lookup/doi/10.1177/1756827716652474.
96. L.Magri, M. P.Juniper, and J. P.Moeck. Sensitivity of the Rayleigh criterion in thermoacoustics. *Journal of Fluid Mechanics*, 882:R1, 2020. doi: 10.1017/jfm.2019.860. URL http://arxiv.org/abs/1910.08040.
97. P.Subramanian, S.Mariappan, R. I.Sujith, and P.Wahi. Bifurcation analysis of thermoacoustic instability in a horizontal Rijke tube. *International Journal of Spray and Combustion Dynamics*, 2(4):325–355, 2011. ISSN 1756-8277. doi: 10.1260/1756-8277.2.4.325.
98. P.Subramanian, R. I.Sujith, and P.Wahi. Subcritical bifurcation and bistability in thermoacoustic systems. *Journal of Fluid Mechanics*, 715:210–238, jan 2013. ISSN 0022-1120. doi: 10.1017/jfm.2012.514. URL http://www.journals.cambridge.org/abstract_S0022112012005149.
99. S.Hermeth, G.Staffelbach, L. Y.Gicquel, V.Anisimov, C.Cirigliano, and T.Poinsot. Bistable swirled flames and influence on flame transfer functions. *Combustion and Flame*, 161(1):184–196, 2014. ISSN 00102180. doi: 10.1016/j.combustflame.2013.07.022. URL http://dx.doi.org/10.1016/j.combustflame.2013.07.022.